Check for updates

Tailoring short-range mobility at donor–acceptor heterointerfaces through small molecules promotes efficient organic solar cells

Top Archie Dela Peña, [ID] †[abcd] Yongmin Luo,†[a] Yulong Hai,†[a] Ruijie Ma, [ID] *[e] Andrew Dolan, [ID] [f] Sepideh Khanmohammadi,[g] Jessica M. de la Perrelle,[fn] Yuanzhi Zheng,[i] Qi Wei,[c] Yao Li,[a] Longfei Jia,[h] Sheena Anne Garcia,[i] King Lun Yeung, [ID] [i] Kateryna Kushnir Friedman,[g] Lyubov V. Titova,[g] Tao Jia,[j] He Yan, [ID] [d] Tak W. Kee, [ID] [f] Wenchao Zhao, [ID] [h] Wei Gao,*[k] Mingjie Li*[cl] and Jiaying Wu [ID] *[am]

Understanding how to optimize the electronic processes and material selections are fundamental to fostering the development of organic solar cells (OSCs). In this report, we identified that small molecule donors (SMDs) could act as nanofillers for the voids in the bulk of photoactive films, which are most prominent at donor–acceptor heterointerfaces due to a higher degree of disorder than molecular domains. Meanwhile, although such more compact heterointerfaces are beneficial in singlet exciton dissociation due to more overlapping electronic wavefunctions, they cannot guarantee device improvements as they also influence the recombination probability. Based on our photophysical analysis, incorporating SMDs with weaker molecular polarizability to occupy these heterointerfaces while preserving the intrinsic delocalization of donor and acceptor singlet excitons is necessary to suppress the sub-nanosecond bimolecular recombination losses, owing to the enhanced short-range mobilities that drive free charges from heterointerfaces towards molecular domains. Herein, this is made possible through the simple fluorination of the molecule B1, generating new B1-derivative SMDs. Uncovering this new design strategy for heterointerfaces is expected to serve as one of the frameworks for the era of >20% efficiency OSCs.

Broader context

Organic solar cells (OSCs) continue to captivate the development of solution-processable and environmentally friendly solar cells. However, as there are an infinite number of ways to optimize OSC devices or molecules, it is essential to construct design strategies to streamline the development towards commercialization. One of the least understood concepts in OCS is the electronic process for donor–acceptor heterointerfaces and the relevant methods to optimize them. Herein, we used the combination of photophysical, thermodynamic, morphological, and electronic characterizations to derive a new

[a] *The Hong Kong University of Science and Technology (Guangzhou), Function Hub, Advanced Materials Thrust, Nansha, Guangzhou, China. E-mail: jiayingwu@ust.hk*

[b] *Nanyang Technological University, School of Materials Science and Engineering, 639798, Singapore*

[c] *The Hong Kong Polytechnic University, Faculty of Science, Department of Applied Physics, Kowloon, Hong Kong, China. E-mail: ming-jie.li@polyu.edu.hk*

[d] *The Hong Kong University of Science and Technology, School of Science, Department of Chemistry, Kowloon, Hong Kong, China*

[e] *Department of Electrical and Electronic Engineering, Research Institute for Smart Energy (RISE), The Hong Kong Polytechnic University, Hong Kong, China. E-mail: ruijie.ma@polyu.edu.hk*

[f] *University of Adelaide, School of Physics, Chemistry & Earth Sciences, Adelaide, South Australia, Australia*

[g] *Worcester Polytechnic Institute, Department of Physics, Worcester, Massachusetts, USA*

[h] *Co-Innovation Center of Efficient Processing and Utilization of Forest Resources, College of Materials Science and Engineering, Nanjing Forestry University, Nanjing, China*

[i] *The Hong Kong University of Science and Technology, School of Engineering, Department of Chemical and Biomolecular Engineering, Kowloon, Hong Kong, China*

[j] *Guangdong Polytechnic Normal University, School of Optoelectronic Engineering, Guangzhou, China*

[k] *Xiamen Key Laboratory of Optoelectronic Materials and Advanced Manufacturing, Institute of Luminescent Materials and Information Displays, College of Materials Science and Engineering, Huaqiao University, Xiamen 361021, China. E-mail: wgao@hqu.edu.cn*

[l] *The Hong Kong Polytechnic University, Photonics Research Institute, Hung Hom, Kowloon, Hong Kong, China*

[m] *The Hong Kong University of Science and Technology, School of Engineering, Department of Chemical and Biological Engineering, Kowloon, Hong Kong, China*

[n] *Future Industries Institute, The University of South Australia, Mawson Lakes, South Australia, 5095, Australia*

† Shares equal contribution.

10164 | *Energy Environ. Sci.*, 2025, **18**, 10164–10179

This journal is © The Royal Society of Chemistry 2025

mechanism for how electronic processes at donor–acceptor interfaces can be refined. Specifically, we proposed the use of small-molecule donors (SMDs) with weak molecular polarizability to occupy the voids at these heterointerfaces. Filling the voids at heterointerfaces ensures a more compact heterointerface for better overlapping electron wavefunction, beneficial to singlet exciton dissociation. Meanwhile, weaker polarizability at heterointerfaces prompts free charges with higher short-range mobilities that drive faster diffusion toward molecular domains, minimizing the probability of encountering opposite charges. Overall, these findings are expected to assist in fostering the era of >20% OSCs.

Introduction

Organic electronics continue to demonstrate great potential as the next-generation solar cell material, thanks to its solution-processability, mechanical flexibility, lightweight, and the absence of toxic heavy metals which may cause risk to humans and the environment.[1] Prior to global industrial adaptation, the economic feasibility of organic solar cell (OSC) technology must be levelized comparable to the $ per kW-h of commercially existing alternative materials. There are many factors to consider and device efficiency is one of those that has received the most attention from the community to date.[2–4] There are several notable works previously published addressing material synthetic designs, device architectures, interlayers, and photo-active layer optimizations (just to name a few).[5–25] The photo-active layer generally consists of electron donors and electron acceptors which collect the solar radiation and convert it to free carriers. Currently, the highest performing OSCs are mostly based on polymer donors and small-molecule acceptors which allows synergistic effects from the morphological stability of polymers and conformational rigidity of small-molecules. Regardless of photo-active layer composition, the majority of previous works are concerned with optimizing pure domain characteristics and associated charge carrier processes,[26–33] which are certainly revolutionary. However, there exists a substantial knowledge deficiency on the functionality and design principles for the donor–acceptor heterointerface,[34] which happens to be the consequence of its complex nature that normally prevents direct characterizations when compared to pure domains. On the other hand, these heterointerfaces are critical to regulate efficient charge carrier processes, thereby requiring urgent attention to continue advancing OSC technology.[34]

As illustrated in Fig. 1a, when polymers are dispersed in solutions, they behave like strings with small crystallite regions and short branched chains. Upon formation of thin films, there will be regions where crystallites from different polymer chains exhibit tightly packed lamellar arrangements with a high degree of order; these are known as pure domains, where most of the existing optimization principles are based.[19,34] Small molecules behave like polymers, although they possess shorter chain lengths, thereby more capable of forming lamellar packing. The amorphous regions consisting of randomly arranged chains, prompting higher free volumes,[35] responsible for donor and acceptor chains to intercalate which regulates intermolecular interactions. A more detailed discussion of the behavior of polymers and small molecules can be found elsewhere.[36–38] As illustrated in Fig. 1b, after the dissociation of singlet excitons is the transport of free charges from donor–acceptor heterointerface towards pure domains. In contrast to inorganic semiconductors possessing covalent (chemical) bonds, the London dispersion forces (LDF) and other weaker physical bonds existing in organic semiconductors can only construct weak molecular coupling. Hence, the charge transport is based on hopping mechanism where the impact of electron–phonon coupling (EPC) is significant. Accordingly, Holstein approximated the free charge transport mobility (μ_{hop}) based on non-negligible EPC, as further elaborated in Note S2.2. Meanwhile, the π-electron cloud polarizing free charge will strain the molecular lattice, causing charge-lattice coupling and forming polarons (i.e., more specifically, small polarons), as illustrated in Fig. 1c. More detailed fundamental discussions are already available from other literature.[39,40] On the other hand, previous studies have successfully demonstrated that stronger polarization can assist the singlet exciton dissociation through increased delocalization from charge screening effects.[41] Intuitively, balancing the trade-off effects of polarization in charge dissociation and free carrier transport sounds reasonable at the limit of single-component and binary-component systems. Meanwhile, organic semiconductors have alleviated lattice matching requirements and thereby can take advantage of the multi-component strategy to fully optimize the polarization effect on free carrier transport without retarding the singlet exciton dissociation efficiency. Likewise, a recent breakthrough was the use of small molecules as guest components,[42] acting as heterointerface void nanofillers. These were found to significantly enhance the stability of OSCs, which is one of the crucial components towards commercialization. Accordingly, the synergistic effects of small molecules on stability and in tuning the donor–acceptor heterointerfaces may hold the key to the next generation of stable and efficient OSCs.

Hence, this work introduces a novel design strategy for donor–acceptor heterointerfaces, refining interface electronic processes. Specifically, newly designed small-molecule donors (SMDs) were added as guest components to primarily occupy the void spaces at the heterointerfaces (illustrated in Fig. 1d and e) while preserving the optoelectronic properties of pure domains. Accordingly, the singlet exciton dissociation efficiency is further enhanced due to more overlapping electronic wavefunctions arising from closer-packed heterointerface assembly. Meanwhile, the guest SMD with weak molecular polarizability is observed to mobilize free holes enabling faster diffusion from heterointerfaces towards donor pure domains. This minimizes free holes exposure time at the heterointerfaces thereby diminishing the probability of immediate recombination losses from Coulombic attraction by re-encountering free electrons residing at acceptor molecules within the heterointerfaces. In addition, the concurrently weaker ability of π-electrons within heterointerfaces to stabilize free carriers is
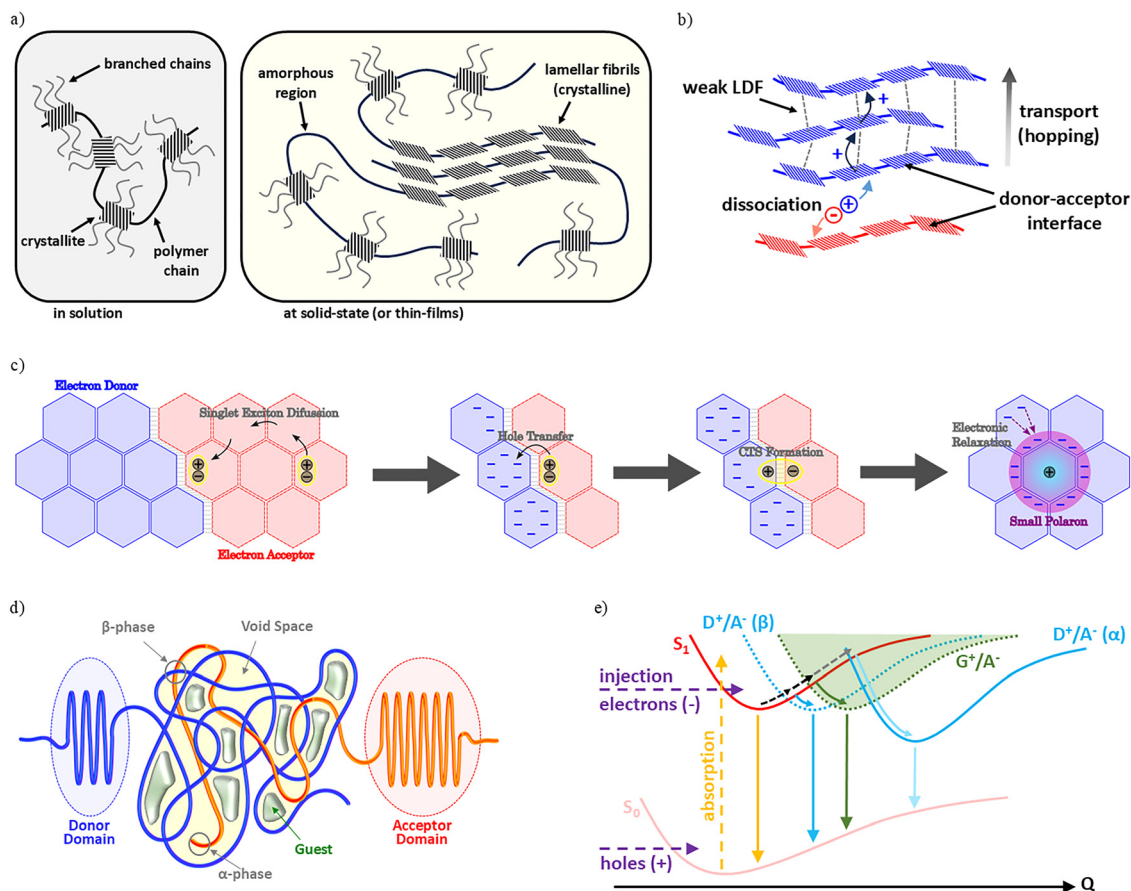
This journal is © The Royal Society of Chemistry 2025

Energy Environ. Sci., 2025, **18**, 10164–10179 | **10165**

Fig. 1 Review of fundamentals and illustration of the proposed multi-component molecular assembly. (a) Polymer (small molecule) chains dispersed in solution and in solid-state. (b) Singlet exciton dissociation and the subsequent hopping-based free carrier transport. (c) Schematics of electronic relaxation from molecular polarization of free holes. (d) Visualization of localized domains and heterointerface with free volumes occupied by guest SMDs. (e) Illustration of charge transfer and fluorescence from D18/L8-BO CTS in α-phase (high in free volume) and in CTS β-phase (closer-packed chains), and SMD/L8-BO heterojunctions. Here, D stands for donor, A for acceptor, and G for guest molecules. In (e), the singlet exciton transition energy diagram is based on the acceptor as the lowest bandgap component, meanwhile, the donor singlet exciton and potential interface states from homointerfaces are excluded for simplicity.

found to construct more pronounced uphill energy landscapes from pure domains to heterointerfaces. Accordingly, free carriers reaching pure domains are electrostatically hindered from migrating back towards recombination-prone heterointerfaces. Overall, this proposed heterointerface design strategy suppresses charge recombination which tunes the device fill factor (FF) and open-circuit voltage (V_{oc}) while also improves the short-circuit current density (J_{sc}), demonstrating device efficiency approaching 20% (certified). Most importantly, this work introduces new perspectives on heterointerface designs and uncovers a deeper comprehension of heterointerface electronic processes which could potentially revolutionize the new era of efficient OSCs.

Improved charge transport with guest SMDs

In this work, a top-notch system D18:L8-BO is selected as the benchmark donor:acceptor system thereby making new design

principles prompting further device improvements to be of practical and significant importance. From here on, heterointerfaces will be referred to as the interface regions where D18 and L8-BO molecular chains are interacting. To enhance free charge transport and suppress recombination losses, this work proposed the concept of molecular polarizability tuning within heterointerfaces. Specifically, a guest component with low molecular polarizability will be introduced to occupy the free volumes within heterointerfaces and modify its electronic nature. Consequently, small molecular donors (SMD) based on B1 and four novel B1 derivatives with different phenylalkyl side chain fluorine functionalization are investigated as the guest component, structures are shown in Fig. 2a (other details are supplied in Fig. S1 and Note S1). There are some empirical observations that electronegative functional groups can decrease the molecular polarizability as a result of increasing the dipole moment.[43] Meanwhile, although this empirical correlation was also observed herein, there remains no clear understanding about this relationship, and it could be subject to further research. From the device efficiency exploration (Fig. 2b, Table S1, and Fig. S2–S4),

10166 | *Energy Environ. Sci.*, 2025, **18**, 10164–10179

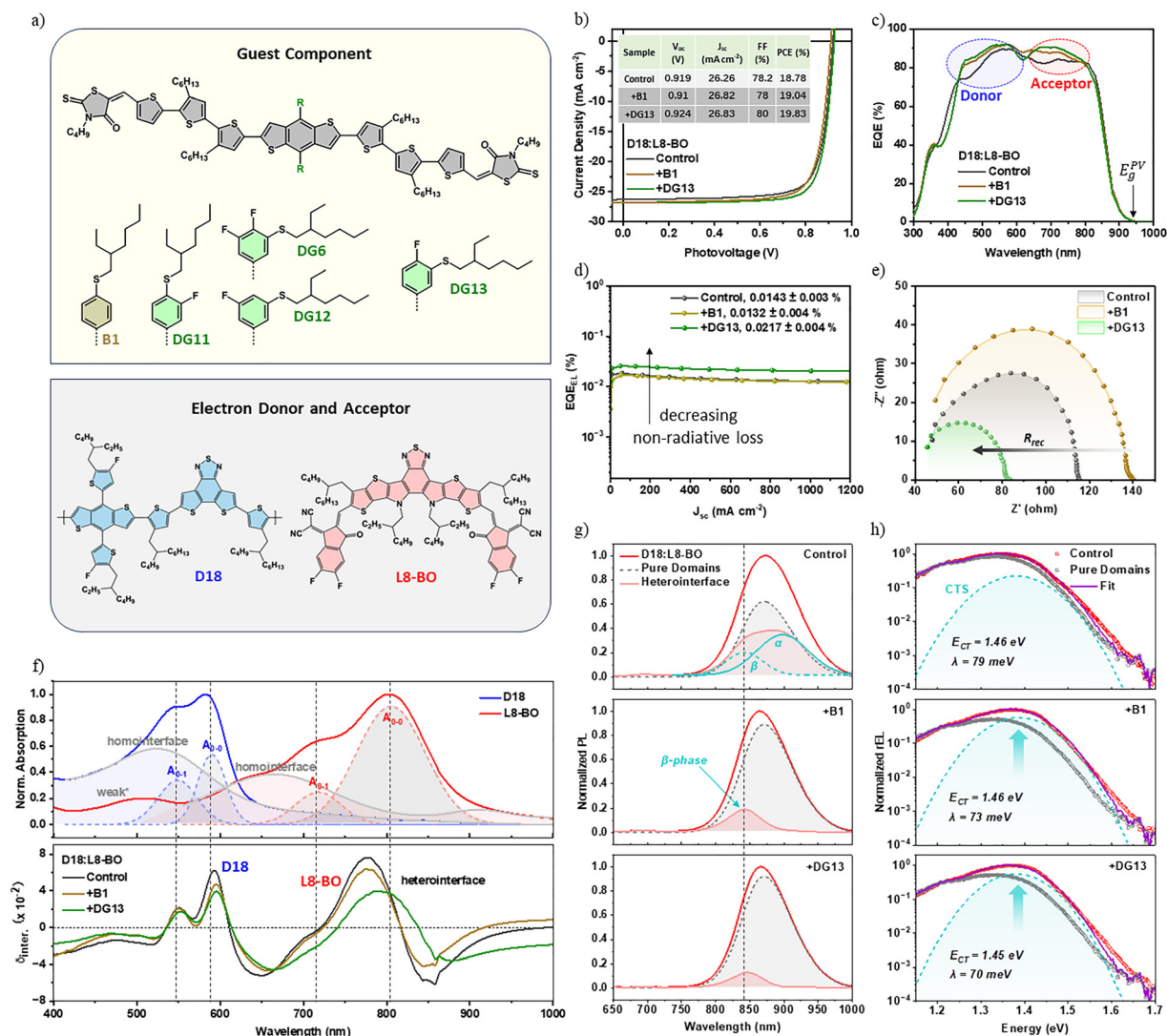This journal is © The Royal Society of Chemistry 2025

Fig. 2 Precursor materials, photovoltaic performance, and optical properties of binary (control) and ternary devices (+B1 and +DG13). (a) Chemical structure of guest small molecule donors (SMDs) (panel above) and the host polymer donor D18 and small molecule non-fullerene acceptor L8-BO (panel below). (b) Current density–voltage curves with inset summarizing the device metrics under 1 Sun illumination in an inert atmosphere. (c) External quantum efficiency (EQE) with highlights corresponding to donor and acceptor-dominated absorption range. (d) Electroluminescence quantum efficiency (EQE_{EL}) against injection current. (e) Nyquist plot from impedance measurement. (f) Normalized absorption of neat D18 and neat L8-BO films deconvoluted based on electronic and vibronic transitions (panel above) and the absorption deviation parameter (δ_{inter}) from the donor–acceptor heterointerface in blend films (panel below). (g) Steady-state photoluminescence (PL) deconvoluted based on L8-BO crystallite and intermixed phase emissions. (h) Reduced electroluminescence (rEL) fitted based on the classical Marcus theory of electron transfer and deconvoluted based on a linear combination approach. Both PL and rEL spectra have been processed with the Jacobian correction factor ($1/E^2$).

B1-ternary only resulted in slight PCE improvement due to lower V_{oc} and fill factor (FF). On the other hand, DG6-ternary suffers from poorer J_{sc} that can be attributed to over-fluorination which is known to cause excessive aggregations.[44] Interestingly, although the corresponding binary SMD:L8-BO devices have much inferior performance (Table S1), ternary devices based on the other fluorinated SMDs (DG11, DG12, and DG13) demonstrate notable improvements with DG13 achieving the best result. Specifically, all the device parameters (*i.e.*, J_{sc}, V_{oc}, and FF) have increased due to improved efficiency for singlet exciton dissociation (η_{diss}) and free charge transport/collection (η_{coll}), leading to a stunning 19.83% PCE (19.48% certified).

The contrast between the resulting V_{oc} and FF of B1 and DG13-based ternaries is further verified by electroluminescence quantum efficiency (EQE_{EL}) and the Nyquist plot (Fig. 2d and e). Higher EQE_{EL} indicates reduced non-radiative recombination loss while a smaller Nyquist radius indicates greater recombination resistance (R_{rec}), both are indicative of enhanced charge transport and suppressed recombination probability. Meanwhile, both B1 and DG13 absorptions peak at around 550–650 nm (Fig. S5), yet there is enhanced external quantum efficiency (EQE) from almost the entire range in the corresponding ternary devices (Fig. 2c) while there are no significant changes in the photovoltaic bandgap ($E_{g,PV}$), as shown in Fig. S6 using FTPS-EQE. Indicatively,

the J_{sc} improvements are mainly due to more favorable singlet excitons dissociation instead of merely complimentary absorption. Likewise, ternary devices display increasing capacitance from the Mott–Schottky plot which indicates easier singlet exciton dissociation (Fig. S7). Additionally, based on performance retention and optical properties (Fig. S5 and Table S2), the ternary blends tend to exhibit enhanced stability upon externally stimulating degradation through thermal aging at 100 °C under dark for 24 up to 500 hours, emphasizing that guest components acting as heterointerface void spaces nanofiller may also foster more stable long-term device performance. On the other hand, the comparable $E_{g,PV}$ between D18:L8-BO binary and ternary with SMDs is an initial indication of unlikelihood for selective molecular alloying with either D18 or L8-BO. Alloyed components are known to modify the frontier molecular energy levels,[45] and thereby the optical response which includes absorption edge. Suggestively, the factors regulating the observed improvements in device metrics are primarily based on heterointerface optimizations. Likewise, the optical, morphological, thermodynamic, and photophysical observations further elaborated in succeeding discussions have ruled out all other models for multi-component systems, as summarized in the review of Gang Li et al.,[46] except for the model where guest molecules occupy the donor–acceptor heterointerfaces. Hence, to validify the proposed heterointerface electronic nature modification through weaker molecular polarizability aided by guest SMDs and to comprehensively understand its influence on charge carrier processes, the following sections will cover the (1) characterization of the pure domains and heterointerfaces through optical and morphological techniques, (2) energetics and electronic properties of guest SMDs, and (3) the dynamics of charge carriers at heterointerfaces.

Before moving forward, it must be noted that heterointerface is a very complex topic for organic electronics due to its innately soft and low-conductive nature which currently prompts challenges for direct morphological characterizations as opposed to crystalline and 2D semiconductor materials. Hence, design strategies for heterointerfaces are lacking while related reports and discussions from previous works are scarce. To gain insights into heterointerface characteristics, optical techniques are currently the most intuitive approach as previously demonstrated,[34,47,48] however, it may unavoidably require advanced analytical treatments and fundamental knowledge for light–matter interactions. In this work, relevant scientific principles will be briefly recalled, but readers are highly encouraged to also take advantage of other materials, including but not limited to.[39,49,50]

SMDs at heterointerface free volumes

Since organic semiconductors are comprised of weak LDF preventing the perturbation of the constituent's electronic nature,[39] the blend absorption spectra (A_{blend}) are decomposed using the equation below (further elaborated in Note S2). In this approach, the spectral difference between blend and neat films can be defined as the absorption deviation parameter ($\delta_{inter.}$), providing a direct representative of the interacting donor and acceptor molecular chains at heterointerfaces.

$$A_{blend}(\lambda) = \sum fA_{neat} + \delta_{inter.}(\lambda)$$

From the binary D18:L8-BO, there is $(-)$ $\delta_{inter.}$ at the homo-interface spectral regions while concurrently a similar magnitude but opposite sign $(+)$ δ_{inter} corresponding to D18 and L8-BO chromophore absorption appears. These chromophore features are slightly energetically shifted, consistent with the property exchange mechanism when molecular chains are interacting but not molecular dissolving each other. Accordingly, the features of $\delta_{inter.}$ describes the known percolation of donor and acceptor molecular chains at amorphous homointerface regions to form the donor–acceptor heterointerface, as mentioned in the introduction. Upon the addition of guest SMDs, there is $(+)$ change in $\delta_{inter.}$ around the absorption peaks of B1 and DG13 chromophores (600–650 nm) when compared to binary D18:L8-BO, consistent with the observations from Raman spectra (Fig. S8), suggesting that both B1 and DG13 as guest components preserved their electronic nature and are unlikely to molecularly alloy with either D18 or L8-BO. Furthermore, there is $(-)$ change in $\delta_{inter.}$ around the D18 and L8-BO heterointerface chromophore features (550–600 nm and 700–850 nm, respectively). Likewise, for DG13-ternary there is a more evident reduction of L8-BO heterointerface chromophore absorption blueshift. From the fitting function definition elaborated in Note S2, these indicate less interacting D18 and L8-BO chains at heterointerfaces which is justified by SMDs occupying the heterointerface free volumes.

The photoluminescence (PL) emission spectra, offering higher sensitivity for heterointerfaces based on former experimental results, can also be decomposed using the same principle as with absorption, shown in Fig. 2g. Specifically, the distinct features relative to neat materials can be regarded as charge transfer state (CTS) emissions.[34,48,51] These CTS are coulombically-attracted electron–hole pairs but spatially separated by few nm distance, electrons in acceptor chains and holes in donor chains. At glance, the CTS PL for D18:L8-BO is quite broad and can be further deconvoluted using two Gaussian functions, arbitrarily assigned here as α- and β-phases. These cannot be attributed to traps as traps are generally not emissive and thereby cannot result in intense PL intensities.[52,53] As formerly observed from fullerene-based systems, the high and low energy CTS emissions depend on the molecular packing density.[39,54] Hence, these two phases are attributed to the different configuration of molecular chains at heterointerfaces, illustrated in Fig. 1d and e. Specifically, chains surrounded by void spaces will suffer large energy loss following the second law of thermodynamics since the entropy is higher with increasing separation distance prompted by void spcaes,[39,55] hence, the charge transfer from D18 and L8-BO chains will require larger energy consumption which results in low energy α-phase emissions. Meanwhile, the β-phase with

high energy emission is then attributed to denser-packed regions around the heterointerfaces wherein electrons and holes from different molecules can readily interact without retarding the system's internal energy. Likewise, this high energy β-phase can concurrently be attributed to the possibility of molecular orbitals hybridization,[56,57] and adiabatic charge transfer,[39] which are both consistent with the mentioned closer-packed D18 and L8-BO chains favoring highly overlapping electronic wavefunctions. Accordingly, upon addition of SMDs forming ternary blends, the β-phase PL remains evident with its intensity and position conservatively kept, indicative that SMDs were not influencing the interaction of D18 and L8-BO chains at β-phase. Meanwhile, the α-phase PL for both ternaries is quenched, conducive to the SMDs occupying the void spaces within α-phase. It is known that charges preferentially direct towards the nearest intermolecular contact,[39] hence the charge transfer from L8-BO singlet excitons to SMDs is more favorable thereby suppressing the α-phase PL. Likewise, the increasing L8-BO pure domain relative PL intensity suggests that CTS geminate recombination probability is suppressed, indicative of more favorable dissociation forming free charges, and is consistent with the SMDs filling up the void spaces in heterointerfaces.

To further understand heterointerfaces, electroluminescence (EL) upon charge injection can probe the emissions from completely relaxed states allowing the extraction of energy (E_{CT}) and reorganization parameter (λ) for CTS following the classical Marcus theory of electron transfer and spectral deconvolution based on linear combination approach.[47,51,58] Referring again to Fig. 1e, the frontier molecular energy levels will be filled with injected free charges wherein recombination can result in photon emission. It must be noted that unlike PL, the EL from CTS (α) can be limited and thereby invisible depending on measurement sensitivity level. This is owing to the small chemical potential ($\Phi \propto 1/r$) caused by void spaces prompting larger separation distance (r) between free electrons and free holes from D18 and L8-BO chains. Hence, charges are funneled towards the competing singlet exciton $S_{1 \to 0}$ emissions. It must be noted that although bipolar injection is possible in type II heterojunctions, the actual device photoactive layer is bulk heterojunction wherein both the donor and acceptor molecules are distributed throughout the junction such that electron/hole injection is not strictly selective to either component. Additionally, strong non-radiative process are expected since EL forms bimolecular CTS wherein 75% are spin-triplets (*i.e.*, spin forbidden for ground state radiative transitions) while the geminate CTS from PL is almost exclusively spin-singlets.[58–60] Hence, singlet exciton EL dominates the spectra in the D18:L8-BO binary device, as shown in Fig. 2h. Meanwhile, the presence of SMDs in ternary devices causes reversal wherein CTS EL dominates. Suggestively, there is enhanced charge transfer through the presence of L8-BO/SMD interfaces, consistent with the mentioned SMD filling up the heterointerface free volumes. The CTS EL herein describes $D18^+/L8\text{-}BO^-$ and $SMD^+/L8\text{-}BO^-$ collectively as they are in energy resonance (Fig. S9). Meanwhile, although E_{CT} is one of the factors influencing the V_{oc}, it fails to explain the V_{oc} of B1- and DG13-ternary devices. Indicatively, there is reduced free

charge recombination probability with DG13-ternary thereby minimizing the recombination-associated energy losses. Additionally, λ are all considerably low, indicative of small nuclear reconfiguration (ΔQ) which can be interpreted as the consequence of reduced Barycenter shifts,[17,39,61] consistent with the mentioned densely-packed D18 and L8-BO chains at β-phase and the closer-packed heterojunctions through SMDs occupying the void spaces.

Meanwhile, it must be clarified that the arbitrary assignments mentioned for α-phase and β-phase for the heterointerfaces are only based on logical analysis, aiming to give a possible explanation for the different responses of the so-called α-phase and β-phase PL and EL. Such α-phase and β-phase notions might open new research avenues through further explorations in the future, but in the context of this paper, they are not significant concerns. In particular, the obvious quenching of the broad CTS PL and the enhanced charge transfer effects from singlet excitons forming CTS EL upon the addition of B1 or DG13 already indicates that these guest components tend to occupy the heterointerfaces.

Simply from these optical and electronic approaches, it can be inferred that both B1 and DG13 as guest components primarily occupy the free volumes within D18:L8-BO heterointerfaces. To further examine these observations, the next section will present morphological and other relevant characterizations.

Nanomorphology

Owing to the soft and complex nature of organic heterointerfaces which generally lack sufficient structural order to be suitable for traditional and more direct morphological characterization methods, this work collectively utilizes scanning probe microscopy, the thermodynamics of mixing, X-ray scattering, conductive and photo-induced force microscopies, and those previously presented optical measurements to interpret the characteristics of heterointerfaces.

From scanning probe microscopy in Fig. S10, it can be observed that both B1 and DG13 have strong self-aggregation tendency. Meanwhile, the large Flory–Huggins interaction parameter (χ) derived from the surface free energies (Fig. S11 and Table S3) indicates that B1 and DG13 are not attractive enough with either D18 or L8-BO to form molecularly alloyed domains. Furthermore, through a more rigorous donor–acceptor ratio-dependent differential scanning calorimetry (DSC) and Nishi–Wang equation for the melting temperature (Fig. S12),[62,63] the extracted interaction parameters (χ) verified the results from contact angle measurements and reaffirmed that both B1 and DG13 do not have sufficient interaction strength with either D18 or L8-BO to form an alloyed molecular domain. Hence, these B1 and DG13 guest molecules will thermodynamically be driven towards the edges of D18 molecular domains and L8-BO molecular domains, which also means occupying the D–A interfaces. Accordingly, low concentrations of B1 and DG13 in the ternary matrix are likely to occupy the free volumes within the D–A heterointerfaces. Consequently, the Urbach parameters extracted from FTPS-EQE with a sensitivity of 10^{-5} to

This journal is © The Royal Society of Chemistry 2025

Energy Environ. Sci., 2025, **18**, 10164–10179 | **10169**

10^{-4} (Fig. S6), mainly corresponding to the characteristics of pure domains,[34] are well kept between binary and ternary systems.

As discussed by Gang Li *et al.*,[46] there are four ternary blend models which depend on the location of the guest components. The most well-known is the alloy model which requires the χ to be nearly zero, indicating very strong interaction with either of the host components, but this is not the case for B1 and DG13 as discussed above through the contact angle and DSC data. Meanwhile, forming independent fibril networks can also be excluded as it is said to require a higher volumetric ratio of the guest component to be added. Another model is when the guest component is embedded in acceptor (or donor) pure domains, forming isolated islands. Both B1 and DG13 are electron donors, so embedding them inside L8-BO acceptor domains will cause holes to be trapped and no way out of the acceptor domain surrounding it which should cause drastic efficiency losses, this case can then be easily ruled out given the observed significant improvements in device performance. On the other hand, embedding B1 or DG13 in D18 domains is more unlikely since χ values indicate a slightly stronger interaction of these guest molecules with the acceptor L8-BO than D18. Meanwhile, in a more conservative sense, the closely similar χ values suggest that D18 and L8-BO attract the guest components with similar strength, so it will be thermodynamically unfavorable if guest components are embedded inside a certain molecular domain. Likewise, the THz photoconductivity dynamics presented in later discussions clearly show a distinct time evolution of charge carriers within D–A heterointerfaces upon the addition of guest components, indicating that B1 and DG13 must be residing at the heterointerfaces to cause such effects. Hence, upon ruling out all other possible ternary blend models, the only possible case that can satisfy all the experimental observations is when B1 and DG13 preferentially occupy the void spaces at D–A heterointerfaces.

The above claims can also be inferred from morphological investigations. From grazing incidence wide-angle X-ray scattering (GIWAXS), the in-plane (IP) lamellar and out-of-plane (OOP) π–π stacking features have been investigated (Fig. 3a and d–f). Based on large crystalline scatterers, primarily representing the pure domains with lamellar packing, there appear
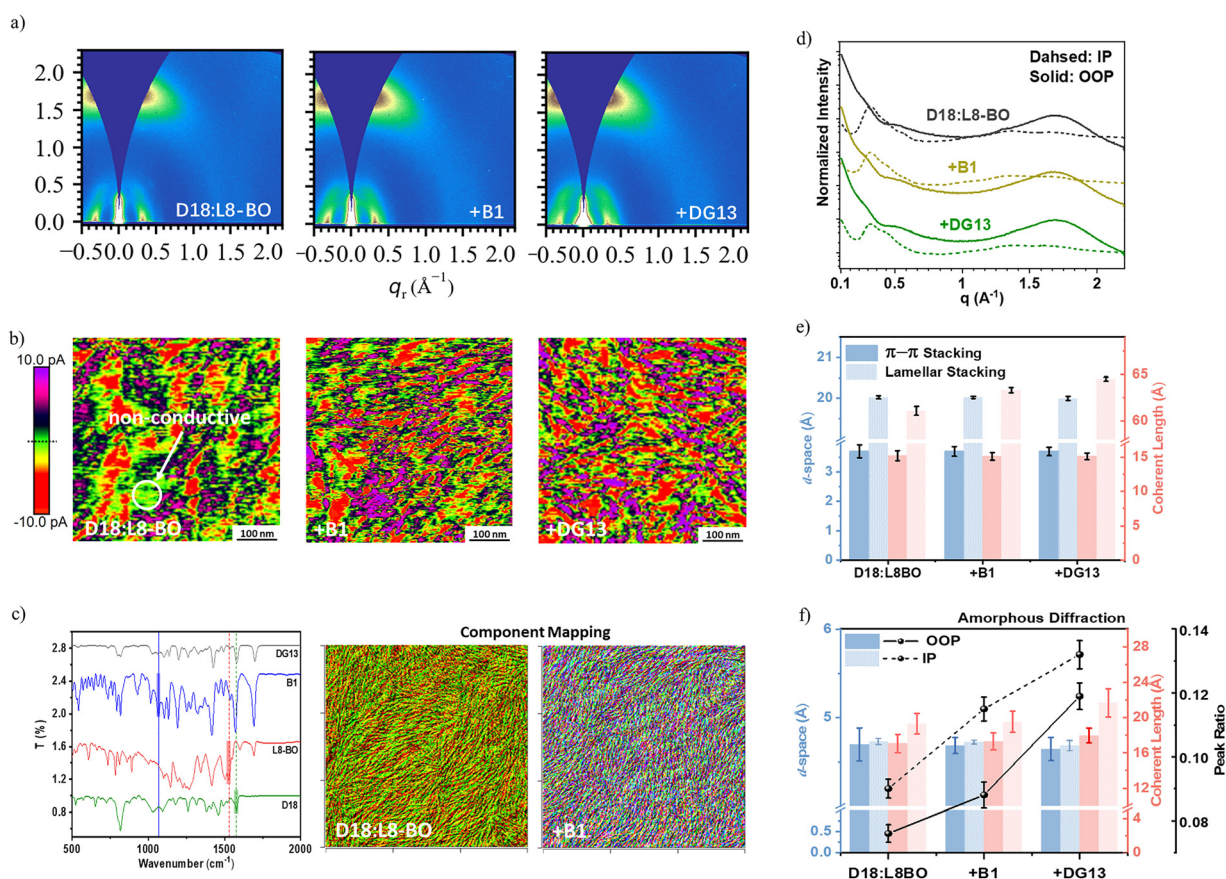

Fig. 3 Heterointerface molecular assembly. (a) Grazing incidence wide angle X-ray scattering (GIWAXS) of blend thin films. (b) Photo-induced force microscopy (PiFM) with reference FTIR transmission spectra of pure materials (left panel) and component mapping in blend films (right panel) from 2 × 2 μm testing area. The PiFM mapping for DG13 ternary is omitted due to lack of clearly distinguishable features compared to D18 and L8-BO while miscibility data suggests it will behave fairly similar to B1. (c) Conductive atomic force microscopy images with red regions showing non-conductive areas which indicates high volume of empty space. (d) The extracted in-plane (IP) and out-of-plane (OOP) line cuts from GIWAXS. (e) Fitted π–π and lamellar stacking features for large crystalline scatterers which represent localized domains. (f) Fitted IP and OOP features from the amorphous diffractions which represent scatterers within the intermixed phase.

to be no significant differences between binary and ternary films (Fig. 3e). However, the amorphous diffractions of the ternary blends exhibit an increasing peak ratio relative to their crystalline domains (Fig. 3f), indicating a higher density of scatterers present within heterointerfaces (*i.e.*, attributed to SMD aggregates). Accordingly, from the amorphous diffractions, the crystal coherence length (CCL) decently increases while the *d*-spacing decreases for ternary films, consistent with the filling up of free volumes within the heterointerfaces through SMDs. In other words, these suggest that SMDs form aggregates with slightly longer coherence lengths than existing D18 (L8-BO) crystallites at heterointerfaces, allowing them to occupy the free volumes which prompts the increasing scattering intensity from amorphous regions. Likewise, from conductive atomic force microscopy mapping (Fig. 3b), the green area for low/non-conductive regions (*i.e.*, between the assemblies of + and − conductance) are smaller for both B1- and DG13-ternary, representing more conductive materials occupying the void spaces within the heterointerfaces. It must be noted that the host donor D18 and host acceptor L8-BO are maintained for all the samples, hence, the less area of low/non-conductive regions at the interface of + and − conductance implies that the addition of B1 or DG13 tends to occupy such interface regions. Furthermore, the photo-induced force microscopy (PiFM) mapping shown in Fig. 3c indicates that SMDs tend to circumambient L8-BO fibrils thereby filling up the free volumes within D18:L8-BO heterointerfaces. This is similar to a recent notable study observing the existence of small aggregates within intermixed amorphous phases.[64]

Furthermore, to more directly verify that both B1 and DG13 indeed occupy such void spaces at heterointerfaces and do not simply splash out from the bulk film after spin casting, quartz crystal microbalance experiments were performed, and results were shown in Fig. S18. Here, an increasing density was obtained upon the addition of either B1 or DG13, which according to the literature,[65,66] further suggests that both these guest molecules can occupy the void spaces and remain there.

Upon consolidating both the optical, thermodynamic, and morphological characterizations presented, it is evident that both the B1 and DG13 as guest components tend to occupy the void spaces within heterointerfaces. This explains the observed J_{sc} improvement for both the ternary systems. Specifically, as electron wavefunctions decay exponentially with distance,[39] the free volumes within heterointerfaces being occupied by SMDs prompts more overlapping donor–acceptor electron wavefunctions. These are fundamental basis for effective tunneling and hopping charge transfer,[39,67,68] beneficial to singlet excitons dissociation. On the other hand, it cannot explain why DG13-ternary also benefits with increasing V_{oc} and FF while B1-ternary incur losses. From earlier discussions, the fluorine functionalized DG13 is synthetically designed to have weaker molecular polarizability than B1. Molecular polarizability is the fundamental basis of electronic relaxation regulating the strength of charge-lattice coupling (or polaronic character),[39] thereby offering different nature of heterointerfaces between B1- and DG13-ternary. To validate

this, the next section will cover the electronic properties and energetics of B1 and DG13.

Tuning the molecular polarizability and energetics

Since the D18 and L8-BO host components are kept, the intrinsic delocalization of photogenerated singlet excitons are retained while guest SMDs modify the electronic nature of heterointerfaces. The chemical structure of B1 and DG13 are presented in Fig. 2a. It can be observed that DG13 benzodithiophene (BDT) donor unit has phenylalkyl side chains functionalized with electronegative fluorine, known to generally decrease molecular polarizability.[43] Indeed, from the results of density functional theory (DFT) calculations shown in Fig. 4a and Table S4, DG13 exhibits a larger dipole moment which pulls the electron cloud thereby reduces the ability to polarize nearby free charges through electronic relaxation of its π-electron system. Take note that this molecular polarization only involves π-electrons and is different from solvation effect since large particles such as polymers and small-molecules in solid-state will not undergo molecular reorientation,[39] unless there is substantially high energy supplied. Likewise, from the DFT polarizability density spatial contribution (Fig. 4b), it can be observed that DG13 has less expanded distribution particularly at the functionalized side chains of BDT indicating its lower polarizability. Furthermore, from molecular dynamics (MD) simulations (Fig. 4c–e), the hole polarization energy (E_{pol,P^+}) of DG13 (0.35 eV) is smaller than B1 (0.91 eV). In other words, there is a larger energy difference from lattice straining arising from stronger free charge-lattice coupling in B1 compared to DG13 complexes.[39] Hence, free holes are less bounded to lattice units around the DG13-ternary heterointerfaces, this should prompt weaker polaronic character thereby enhancing the free holes short-range mobility for transport towards D18 pure domains,[39] and likewise minimizes the free holes exposure time at heterointerfaces.

Aside from free carrier mobilities, the relaxation of π-electron clouds toward free holes must be driven by energy stabilization, following the laws of thermodynamics, which prompts reduction in the energy of the charge carriers. To verify this effect, B1 and DG13 solutions were prepared in dilute concentration using polar and non-polar solvents. Herein, polar solvents are used to represent the effect of highly polarizable mediums while non-polar solvents for weakly polarizable mediums. From the absorption spectra shown in Fig. 4f, it can be observed that polar solvents polarizing the intrinsic free carriers within both B1 and DG13 imparts redshifted absorptions, consistent with the mentioned energy reduction as result of charge stabilization. For the actual thin films, the environment surrounding free carriers are the molecular assemblies of B1 and DG13 molecules themselves. In dilute solution state, the polarization from the π-electrons of surrounding B1 (DG13) molecules are insignificant due to the lack of molecular packing. However, in solid-state, B1 (DG13)

This journal is © The Royal Society of Chemistry 2025

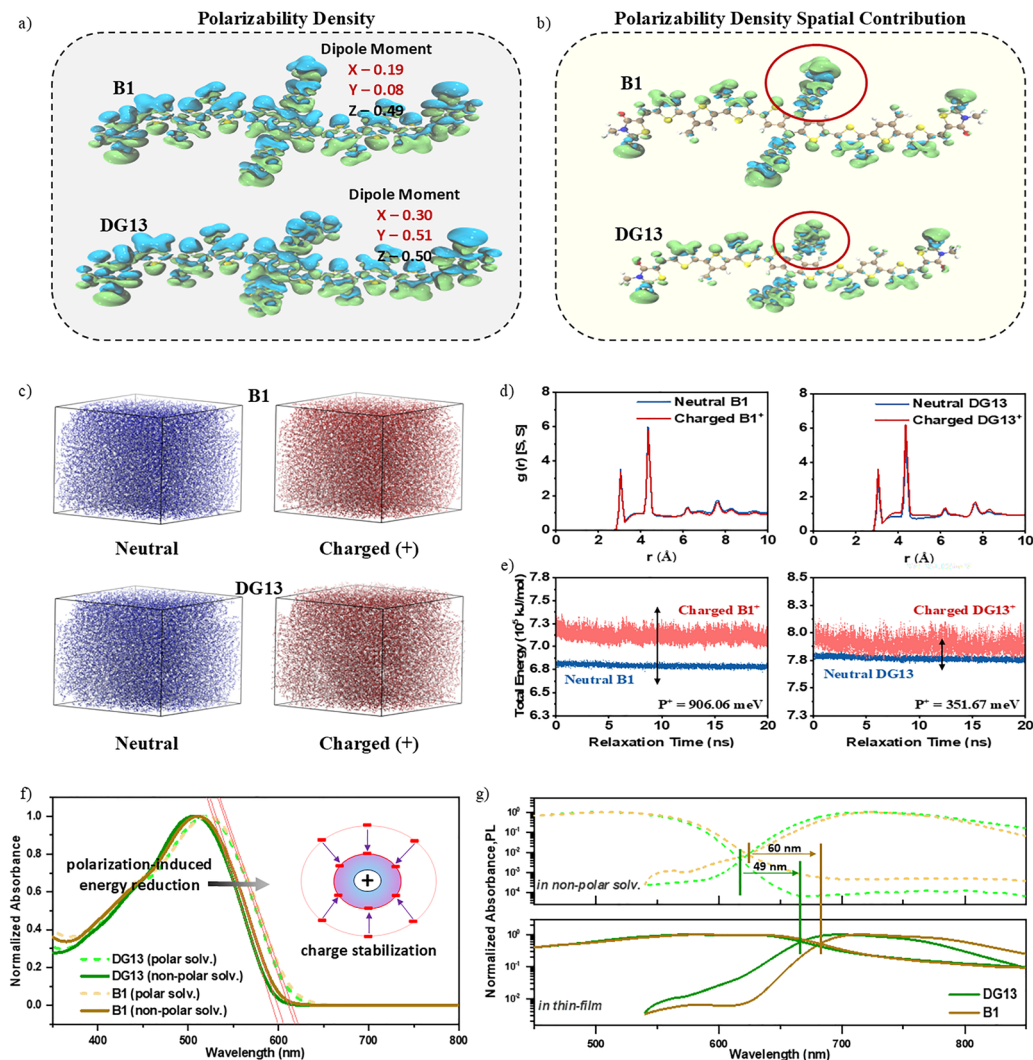*Energy Environ. Sci.*, 2025, **18**, 10164–10179 | **10171**

Fig. 4 Density functional theory (DFT) calculations and molecular dynamics (MD) simulations. (a) DFT polarizability density. (b) DFT polarizability spatial distribution. (c) MD phase equilibrium of neutral (blue) and charged (red) molecules. (d) MD radial distribution function. (e) MD statistical total energy in 20 ns with the average difference shown as P^+. (f) Environment polarization dependence of absorption onset. (g) Environment polarization dependence of adiabatic transition energy. The corresponding dipole moments and static polarizability in x, y, and z directions are shown in Table S4. The concentration of solutions used for absorption and PL were diluted at 0.5 mg ml^{-1}, o-dichlorobenzene was used as the polar solvent while toluene as the non-polar solvent.

molecules are denser packed allowing their electron cloud to interact with nearby molecules/charges. From Fig. 4g, lower adiabatic transition energies were observed from both B1 and DG13 in thin films compared with diluted solutions using a non-polar solvent. Accordingly, the impact of molecular polarization through π-electrons is further confirmed to impart reduction in charge carrier energy. Likewise, the redshift is larger for B1 despite previous morphological data presented indicates that DG13 have slightly stronger aggregation property than B1. This is consistent with the result of DFT and MD indicating that B1 exhibits a larger polarization energy (*i.e.*, more polarizable) than DG13. Hence, the energy landscape from pure domains to DG13-ternary heterointerfaces will be more energetically uphill than B1-ternary. This creates an energy barrier for free carriers at pure domains to migrate back towards the recombination-prone heterointerfaces.

In this section, DG13 is shown to have weaker molecular polarizability than B1 which is demonstrated to mobilize free holes, consistent to the Holstein approximation. In other words, free holes at DG13 units cause less lattice straining and thereby weaker charge-lattice coupling which favors hopping transport from one molecular site to another.[39] Accordingly, DG13-occupied heterointerface free volumes comes with more mobile free holes subsequent to singlet excitons dissociation. This allows faster free carrier diffusion towards D18 pure domains, thereby reducing the holes exposure time at the heterointerfaces. Heterointerfaces are recombination-prone regions due to the high chance of encountering oppositely charged carriers which through Coulombic attraction can facilitate recombination. Meanwhile, the weaker molecular polarizability of DG13 also weakens the ability of its π-electrons to stabilize free holes through electronic relaxation.[39] This electrostatic stabilization

10172 | *Energy Environ. Sci.*, 2025, **18**, 10164–10179

This journal is © The Royal Society of Chemistry 2025

is demonstrated here to decrease the energy level of charge carriers. Accordingly, free holes reaching D18 pure domains through diffusion will experience greater electrostatic energy barrier for migrating back towards heterointerfaces in DG13-ternary. Both the enhanced free carrier short-range mobility and the resulting energy landscape can facilitate the suppression of recombination losses, justifying the observed FF and V_{oc} between B1- and DG13-ternary. To further understand these effects, the dynamics of charge carriers are investigated in the next section.

Suppressed recombination losses at heterointerfaces

Ultrafast spectroscopic techniques are inevitable to gain insights into the charge carrier processes. Herein, various ultrafast techniques will be used to validate the effects of the proposed heterointerface design principles in the charge carrier processes and to confirm consistency with observed changes in photovoltaic performance. Specifically, for pump–probe transient absorption spectroscopy (TAS), the white light probe can monitor the charge population density while THz probe is for photoconductivity, as elaborately described elsewhere.[69] Photoconductivity is simply the dot product of population and short-range mobility (SRM), making the THz probe provide insights into mobility dynamics. It must be noted that the typically reported bulk mobilities (e.g., from space-charge-limited current) correspond to long-range transport while SRM is specific to charges transferring within nearby molecules. Hence, SRM is more meaningful in understanding the nature of free charge carriers immediately following their generation at the heterointerfaces.[69]

Pseudo 2D maps of neat and blend films TAS and the corresponding spectral line cuts were shown in Fig. S13, S14 and Fig. 5a, respectively. In this work, charge carrier dynamics will be mostly based on selective L8-BO excitation since it is the lowest bandgap component, thereby preventing simultaneous donor and acceptor excited states bleaching which allows more simplified data analysis and clearer overview of the charge carrier processes at heterointerfaces. Nevertheless, the free charge recombination at heterointerfaces is in principle independent of whether their origin is acceptor or donor singlet excitons. Upon selective L8-BO excitation with 800 nm pump laser, it can be observed that the emerging free charge photobleach at 500–600 nm correspond well with the absorption spectra of D18, suggesting that hole polarons tend to migrate in D18 pure domains for both binary and SMD-incorporated ternary samples. However, these free charge photobleach features are highly convoluted with the L8-BO singlet exciton photo-induced absorption (PIA). As shown in Fig. 5b and Fig. S13, the L8-BO singlet exciton features are mainly absent at 980–1200 nm, hence, this range was used in this work to more explicitly probe the dynamics of free charges based on their PIA emerging at 980–1020 nm. Furthermore, to more accurately understand the TAS results, the intensities of free charge photobleaching intensity and kinetics were normalized to the

maximum ground state bleaching (GSB) of L8-BO singlet excitons, as shown in Fig. 5c. It can be observed that DG13-ternary displays the highest free charge bleaching intensity at the dissociation-recombination equilibrium time range (i.e., around 50–100 ps). Indicatively, the exciton dissociation is enhanced and/or the free charge recombination is suppressed, which are both consistent with the observed improvements in device J_{sc}, FF, and V_{oc}. On the other hand, the equilibrium intensity for B1-ternary is even slightly lower compared to the binary D18:L8-BO.

To decouple the dissociation and recombination factors, both influencing the equilibrium intensity of B1-ternary, a third beam as low energy push pulse was used to temporarily dissociate trapped excitons (i.e., excitons that remains undissociated and likely to contribute to geminate losses), shown in Fig. 5e. The 965 nm push pulse absorbed by the broad near-IR excited state absorption comprised of both singlet and polaron states.[70] The push pulse arrived 10 ps after the initial excitation by the 800 nm pump pulse, after prompt exciton dissociation is expected to have occurred.[70,71] The push pulse induced an increase in the polarons photobleach (650–850 nm and 550–600 nm) and further polaron absorption (900–950 nm). It must be noted that the push wavelength chosen is below the bandgap and does not cause any ground state excitation while the relative push-induced photobleaching among the samples can be consistently observed at various pump excitation fluence (Fig. S15). Hence, the increased photobleaching between 650–850 nm is a result localized singlet excitons separation over multiple L8-BO chromophores, which then increase the photobleaching at 550–600 nm arising from push induced hole transfer from either polaron or singlet excited states. As shown in Fig. 5e, the push pulse induced exciton dissociation is reduced when progressing from the binary blend to the ternary blend films. The reduced push induced dissociation indicates that the population of trapped singlet excitons is effectively suppressed by the addition of B1 and DG13 for the ternary blends. It is also evident from kinetics plot (Fig. 5f) wherein the initial push-induced intensity response for the ternary blends is comparably lower (i.e., suggestive of enhanced dissociation efficiency) while for the binary blend the response is higher. Accordingly, the lower equilibrium intensity of B1-ternary previously seen from TAS can then be attributed to free charge recombination losses. To further confirm it, the free charge PIA recombination kinetics can be fitted through sum of exponentials (Fig. 5d). The first exponential component can be understood as upfront recombination after free charges are generated at heterointerfaces while the second component can be taken to represent those free charges that already have diffused towards pure domains but have migrated back to heterointerfaces wherein they re-encounter opposite charges. For both components, a prolonged decay lifetime is obtained for DG13-ternary while shortened lifetimes for B1-ternary. The first lifetime component is consistent with the mentioned hypothesis based on the high molecular polarizability of B1, causing stronger charge-lattice coupling and relaxation immediately following the generation of free charges at heterointerfaces, as also defined by Holstein approximations. In other words, the free
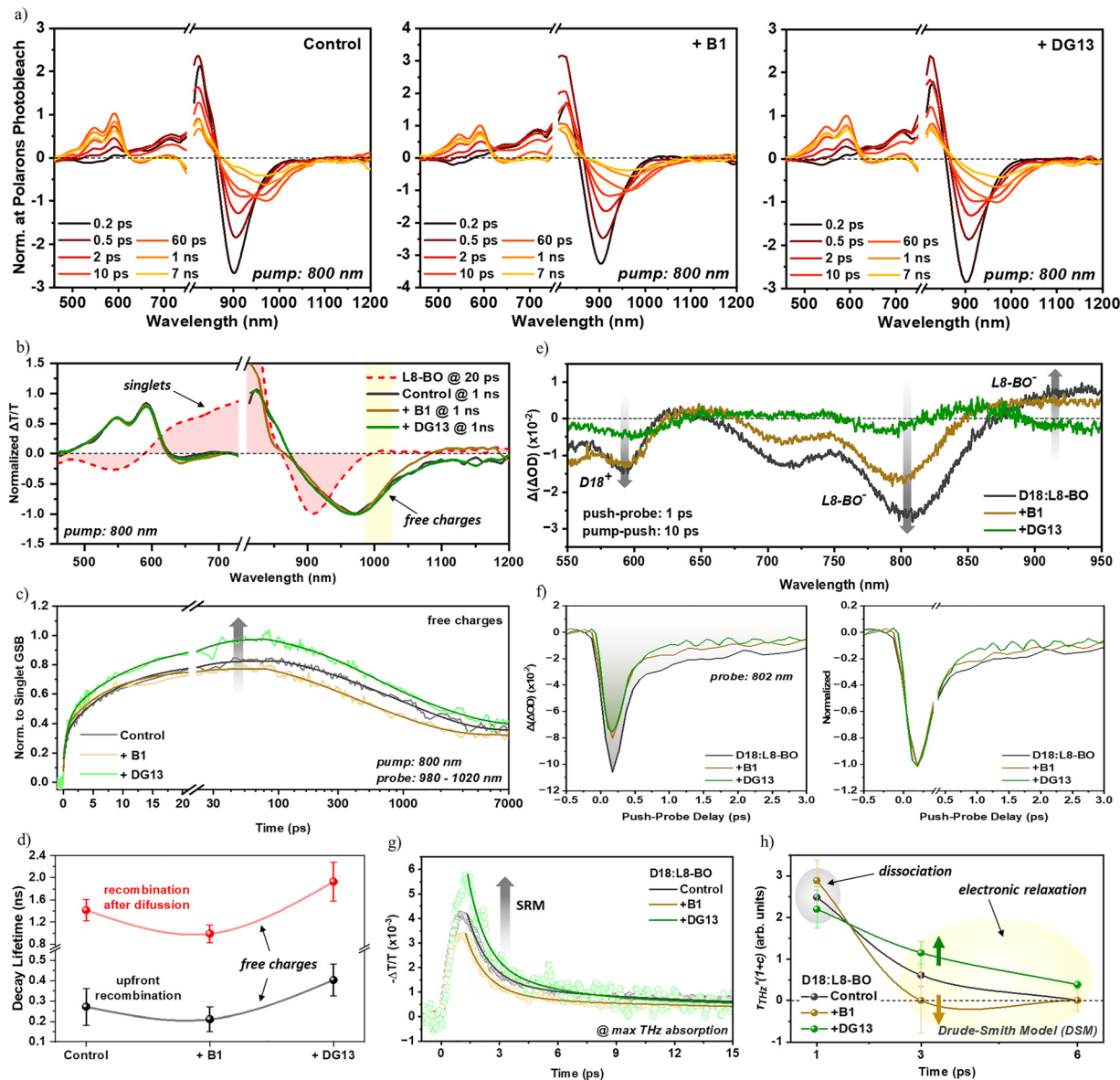
This journal is © The Royal Society of Chemistry 2025

Energy Environ. Sci., 2025, **18**, 10164–10179 | **10173**

Fig. 5 Characteristics of charge carriers. (a) Spectral line cuts from transient absorption spectroscopy (TAS) with 800 nm laser excitation sources at 0.5 μJ cm^{-2} fluence. (b) Representative TAS spectral line cuts for neat L8-BO and donor−acceptor blended films. (c) Kinetics plot of the free charges probed at 980−1020 nm range. (d) Fitted recombination lifetimes through sum of exponentials for the kinetics of free charges at 980−1020 nm probe range. (e) Pump−push−probe TAS with 800 nm pump wavelength and 965 nm push wavelength. Each of the spectra has been normalized to the L8-BO singlet exciton ground state bleaching (GSB) from the corresponding pump−probe measurement. (f) Kinetics of push-induced electron polarons normalized to pump−probe L8-BO singlet exciton GSB (left panel) and normalized to maximum (right panel). (g) Terahertz photoconductivity dynamics measured at maximum terahertz absorption with 800 nm pump excitation. (h) Drude-Smith model fitting of the complex photoconductivity spectra with real part ($\Delta\sigma_1$) and imaginary part ($\Delta\sigma_2$) to extract the SRM at different time domains.

charges in B1-ternary are relatively more stagnant after they are formed at heterointerfaces, this increases their probability of re-encountering opposite charges before even reaching pure domains. The second lifetime component is consistent with the reduced probability of free charges reaching pure domains to migrate back towards recombination-prone heterointerfaces in DG13-ternary, attributed to the more uphill domain-to-interface energy landscape as inferred in earlier discussions.

Ging back with the push-induced dynamics, at <0.5 ps the normalized kinetics (Fig. 5f) show comparable relaxation of some push-induced free charges back to the ground state among all the samples. However, at >0.5 ps push–probe delay, the DG13-ternary have faster relaxation back to unperturbed state despite the push-induced free charge generation is similar to B1-ternary. This can be an initial indication that free charges in DG13-ternary intermixed phase have higher short-range mobilities becoming more evident as time progresses after dissociation. To further verify it, photoconductivity dynamics through THz spectroscopy is performed. From the device metrics (Table S1), the free charge generation between B1 and

10174 | *Energy Environ. Sci.*, 2025, **18**, 10164–10179

This journal is © The Royal Society of Chemistry 2025

DG13-ternaries are comparable, factoring out the effect of the population density thereby the relative initial photoconductivity can be a relative basis for SRM. Upon free charge generation, a much higher THz intensity is observed for DG13-ternary (Fig. 5g), indicative of more mobile free charges emerging at the heterointerfaces. On the other hand, even lower intensity is displayed by B1-ternary despite its more efficient free charge generation efficiency than the binary D18:L8-BO, implying more localized free charges at heterointerfaces. Furthermore, the non-zero real components in the complex photoconductivity plots confirm that the THz dynamics is mainly probing the free charges (Fig. S16), given that singlet excitons absorption is far from the THz region.[72] Using the Drude-Smith model (DSM),[69,73] and based on uniform charge effective mass, the effective SRM will be proportional to $\tau_{THz} \times (1 + c)$,[69] where τ_{THz} and c are fitting parameters corresponding to scattering time and localization parameter, respectively. The results of DSM fits at different time domains were shown in Fig. S16 and Fig. 5h. The SRM is observed to immediately decrease a few ps after charge dissociation which is expected as the result of π-electron cloud polarizing free charges causing charge-lattice coupling and relaxation (Fig. 5h), supporting the Holstein approximations. Interestingly, the decrease in SRM is slower for DG13-ternary while more rapid for the B1-ternary, confirming the hypothesized impacts of guest SMD's molecular polarizability in tuning the electronic nature of heterointerfaces. Accordingly, the generated free charges in DG13-ternary are more mobilized, reducing their exposure time at the recombination-prone heterointerface regime, thereby minimizing the chance of re-encountering opposite charges that prompts bimolecular recombination losses. From spin statistics, 75% of states generated from bimolecular recombination are of triplet character which is known to be a prime factor in the non-radiative energy losses for OSCs.[74] Consistently, DG13-ternary demonstrates the highest EQE_{EL} (Fig. 2d) which translates to reduced non-radiative energy loss and thereby explains its enhanced device FF and V_{oc}.

Meanwhile, the different time evolution of free carrier mobility and dynamics from THz photoconductivity experiments, which is sensitive to free carriers at heterointerfaces, further validates the earlier claim that B1 and DG13 must be preferentially occupying the void spaces at heterointerfaces and thereby capable of prompting different dynamic response for charge carriers at such heterointerfaces. With all the other known models of ternary systems,[46] these effects are plausible only when the guest components are in heterointerfaces.

For a side note, both B1 and DG13 form a cascading energy landscape as indicated by photoelectron spectroscopy (Fig. S19), which previous works verified to promote slower but more efficient singlet exciton dissociation process.[75] This is in-line with the improvements in the J_{sc} observed in this work. However, such a cascading energy landscape fails to explain the different trends in free carrier recombination dynamics and the evolution of short-range mobility at heterointerfaces, which are found to strongly correlate with the different response of device FF upon the addition of B1 and DG13. Hence, the concept of tuning the heterointerface charge-lattice coupling through

molecular polarizability is a new design principle that complements existing knowledge thereby fostering the era of more efficient OSCs.

Summary and conclusion

This work takes advantage of a recent breakthrough in advancing more stable OSCs with the use of SMDs as heterointerface void nanofillers, which opens new avenues in designing new materials and device engineering ideas for OSCs to reach commercial standards. However, it was found herein that these SMDs may not cause any beneficial impacts on photovoltaic efficiency, and may even prompt inferior performance, when the molecular polarizability of SMDs is not properly designed. Herein, the singlet exciton dissociation efficiency based on a star system D18:L8-BO is further improved through the closer-packed molecular chain assemblies at heterointerfaces with SMDs. However, the resulting changes in device V_{oc} and FF are found to compensate for such advantages unless the SMDs regulating the electronic nature at donor–acceptor heterointerfaces come with low molecular polarizability. This is found essential to facilitate higher short-range mobility and more energetic states at heterointerfaces, favoring free carrier diffusion towards pure domains and minimizing the chances of back recombination. Uncovering this design principle for heterointerfaces enables enhanced device stability with superior singlet exciton dissociation and suppressed recombination losses, leading to a certified efficiency of nearly 20%. Overall, the findings in this work are expected to serve as a foundation for future materials and device innovations.

Methods

Details are provided in the SI.

Author contributions

Conceptualization: T. A. Dela Peña, R. Ma, and J. Wu; methodology: T. A. Dela Peña and R. Ma; investigation: T. A. Dela Peña, Y. Luo, Y. Hai, R. Ma, A. Dolan, S. Khanmohammadi, J. M. De La Perrelle, Q. Wei, Y. Li, L. Jia, S. A. Garcia, K. L. Yeung, K. K. Friedman, L. Titova, T. Jia, H. Yan, T. Kee, W. Zhao, W. Gao, M. Li, and J. Wu; writing – original draft: T. A. D. P.; writing – editing & revisions: T. A. Dela Peña, R. Ma, M. Li, J. Wu; supervision: M. Li and J. Wu; and funding acquisition: M. Li and J. Wu.

Conflicts of interest

The authors declare no competing financial interests.

Data availability

All the data generated in this study are included in the Article and its supplementary information (SI). Supplementary information:

Methods, supplementary figures, supplementary tables, supplementary discussions, and supplementary notes. See DOI: **https://doi.org/10.1039/d5ee05342k**.

Raw files or additional data relevant to the paper are available from the corresponding author upon reasonable request.

Acknowledgements

References

1 T. A. Dela Peña, R. Ma, W. Gao, Z. Wei, H. Zhou, J. Wu, A. Facchetti and G. Li, Advancing organic photovoltaics processed from green-solvents: From characterization methods to optimization strategies, *EnergyChem*, 2025, **7**, 100162.

2 A. Armin, W. Li, O. J. Sandberg, Z. Xiao, L. Ding, J. Nelson, D. Neher, K. Vandewal, S. Shoaee, T. Wang, H. Ade, T. Heumüller, C. Brabec and P. Meredith, A History and Perspective of Non-Fullerene Electron Acceptors for Organic Solar Cells, *Adv. Energy Mater.*, 2021, **11**, 2003570.

3 A. Karki, A. J. Gillett, R. H. Friend and T. Q. Nguyen, The path to 20% power conversion efficiencies in nonfullerene acceptor organic solar cells, *Adv. Energy Mater.*, 2021, **11**, 2003441.

4 W. Yang, W. Wang, Y. Wang, R. Sun, J. Guo, H. Li, M. Shi, J. Guo, Y. Wu, T. Wang, G. Lu, C. J. Brabec, Y. Li and J. Min, Balancing the efficiency, stability, and cost potential for organic solar cells via a new figure of merit, *Joule*, 2021, **5**, 1209–1230.

5 A. Classen, C. L. Chochos, L. Lüer, V. G. Gregoriou, J. Wortmann, A. Osvet, K. Forberich, I. McCulloch, T. Heumüller

6 and C. J. Brabec, The role of exciton lifetime for charge generation in organic solar cells at negligible energy-level offsets, *Nat. Energy*, 2020, **5**, 711–719.

6 Y. Zhou, M. Li, H. Lu, H. Jin, X. Wang, Y. Zhang, S. Shen, Z. Ma, J. Song and Z. Bo, High-Efficiency Organic Solar Cells Based on a Low-Cost Fully Non-Fused Electron Acceptor, *Adv. Funct. Mater.*, 2021, **31**, 2101742.

7 Y. Wei, J. Yu, L. Qin, H. Chen, X. Wu, Z. Wei, X. Zhang, Z. Xiao, L. Ding, F. Gao and H. Huang, A universal method for constructing high efficiency organic solar cells with stacked structures, *Energy Environ. Sci.*, 2021, **14**, 2314–2321.

8 Z. Jia, S. Qin, L. Meng, Q. Ma, I. Angunawela, J. Zhang, X. Li, Y. He, W. Lai, N. Li, H. Ade, C. J. Brabec and Y. Li, High performance tandem organic solar cells *via* a strongly infrared-absorbing narrow bandgap acceptor, *Nat. Commun.*, 2021, **12**, 178.

9 J. Cheng, C. Guo, L. Wang, Y. Fu, D. Li, C. Chen, Z. Gan, Y. Sun, D. Liu, W. Li and T. Wang, Device engineering of non-fullerene organic photovoltaics with extrapolated operational T80 lifetime over 45 000 h in air, *Joule*, 2024, **8**(8), 2250–2264.

10 L. Wang, C. Chen, Y. Fu, C. Guo, D. Li, J. Cheng, W. Sun, Z. Gan, Y. Sun, B. Zhou, C. Liu, D. Liu, W. Li and T. Wang, Donor–acceptor mutually diluted heterojunctions for layer-by-layer fabrication of high-performance organic solar cells, *Nat. Energy*, 2024, **8**, 208–218.

11 Z. Chen, J. Zhu, D. Yang, W. Song, J. Shi, J. Ge, Y. Guo, X. Tong, F. Chen and Z. Ge, Isomerization strategy on a non-fullerene guest acceptor for stable organic solar cells with over 19% efficiency, *Energy Environ. Sci.*, 2023, **16**, 3119–3127.

12 L. Kong, Z. Zhang, N. Zhao, Z. Cai, J. Zhang, M. Luo, X. Wang, M. Chen, W. Zhang, L. Zhang, Z. Wei and J. Chen, In Situ Removable Additive Assisted Organic Solar Cells Achieving Efficiency over 19% and Fill Factor Exceeding 81%, *Adv. Energy Mater.*, 2023, **13**, 2300763.

13 G. Ding, T. Chen, M. Wang, X. Xia, C. He, X. Zheng, Y. Li, D. Zhou, X. Lu, L. Zuo, Z. Xu and H. Chen, Solid Additive-Assisted Layer-by-Layer Processing for 19% Efficiency Binary Organic Solar Cells, *Nano-Micro Lett.*, 2023, **15**, 92.

14 D. Li, N. Deng, Y. Fu, C. Guo, B. Zhou, L. Wang, J. Zhou, D. Liu, W. Li, K. Wang, Y. Sun and T. Wang, Fibrillization of Non-Fullerene Acceptors Enables 19% Efficiency Pseudo-Bulk Heterojunction Organic Solar Cells, *Adv. Mater.*, 2023, **35**, 2208211.

15 S. Guan, Y. Li, C. Xu, N. Yin, C. Xu, C. Wang, M. Wang, Y. Xu, Q. Chen, D. Wang, L. Zuo and H. Chen, Self-Assembled Interlayer Enables High-performance Organic Photovoltaics with Power Conversion Efficiency Exceeding 20%, *Adv. Mater.*, 2024, **36**, 2400342.

16 Y. Jiang, S. Sun, R. Xu, F. Liu, X. Miao, G. Ran, K. Liu, Y. Yi, W. Zhang and X. Zhu, Non-fullerene acceptor with asymmetric structure and phenyl-substituted alkyl side chain for 20.2% efficiency organic solar cells, *Nat. Energy*, 2024, **9**, 975–986.

17 L. Zuo, S. B. Jo, Y. Li, Y. Meng, R. J. Stoddard, Y. Liu, F. Lin, X. Shi, F. Liu, H. W. Hillhouse, D. S. Ginger, H. Chen and

10176 | *Energy Environ. Sci.*, 2025, **18**, 10164–10179

This journal is © The Royal Society of Chemistry 2025

A. K.-Y. Jen, Dilution effect for highly efficient multiple-component organic solar cells, *Nat. Nanotechnol.*, 2022, **17**, 53–60.

18 M. Günther, N. Kazerouni, D. Blätte, J. D. Perea, B. C. Thompson and T. Ameri, Models and mechanisms of ternary organic solar cells, *Nat. Rev. Mater.*, 2023, **8**, 456–471.

19 T. A. Dela Peña, R. Ma, Y. Luo, Z. Xing, Q. Wei, Y. Hai, Y. Li, S. A. Garcia, K. L. Yeung, T. Jia, K. S. Wong, H. Yan, G. Li, M. Li and J. Wu, Manipulating the Charge Carriers Through Functionally Bridged Components Advances Low-Cost Organic Solar Cells with Green Solvent Processing, *Adv. Energy Mater.*, 2024, **14**, 2303169.

20 C. Han, J. Wang, S. Zhang, L. Chen, F. Bi, J. Wang, C. Yang, P. Wang, Y. Li and X. Bao, Over 19% Efficiency Organic Solar Cells by Regulating Multidimensional Intermolecular Interactions, *Adv. Mater.*, 2023, **35**, 2208986.

21 B. Zou, W. Wu, T. A. Dela Peña, R. Ma, Y. Luo, Y. Hai, X. Xie, M. Li, Z. Luo, J. Wu, C. Yang, G. Li and H. Yan, Step-by-Step Modulation of Crystalline Features and Exciton Kinetics for 19.2% Efficiency Ortho-Xylene Processed Organic Solar Cells, *Nano-Micro Lett.*, 2023, **16**, 30.

22 L. Zhan, S. Li, T.-K. Lau, Y. Cui, X. Lu, M. Shi, C.-Z. Li, H. Li, J. Hou and H. Chen, Over 17% efficiency ternary organic solar cells enabled by two non-fullerene acceptors working in an alloy-like model, *Energy Environ. Sci.*, 2020, **13**, 635–645.

23 F. Liu, L. Zhou, W. Liu, Z. Zhou, Q. Yue, W. Zheng, R. Sun, W. Liu, S. Xu, H. Fan, L. Feng, Y. Yi, W. Zhang and X. Zhu, Organic Solar Cells with 18% Efficiency Enabled by an Alloy Acceptor: A Two-in-One Strategy, *Adv. Mater.*, 2021, 2100830.

24 Y. Wei, N. Liang, W. Jiang, T. Zhai and Z. Wang, Rylene-Fullerene Hybrid an Emerging Electron Acceptor for High-Performing and Photothermal-Stable Ternary Solar Cells, *Small*, 2022, **18**, 2104060.

25 M. Jiang, H.-F. Zhi, B. Zhang, C. Yang, A. Mahmood, M. Zhang, H. Y. Woo, F. Zhang, J.-L. Wang and Q. An, Controlling Morphology and Voltage Loss with Ternary Strategy Triggers Efficient All-Small-Molecule Organic Solar Cells, *ACS Energy Lett.*, 2023, **8**, 1058–1067.

26 Y. Wang, J. Yu, R. Zhang, J. Yuan, S. Hultmark, C. E. Johnson, N. P. Gallop, B. Siegmund, D. Qian, H. Zhang, Y. Zou, M. Kemerink, A. A. Bakulin, C. Müller, K. Vandewal, X.-K. Chen and F. Gao, Origins of the open-circuit voltage in ternary organic solar cells and design rules for minimized voltage losses, *Nat. Energy*, 2023, **8**, 978–988.

27 Y. Yan, Y. Zhang, Y. Liu, Y. Shi, D. Qiu, D. Deng, J. Zhang, B. Wang, M. A. Adil, K. Amin, W. A. Memon, M. Wang, H. Zhou, X. Zhang and Z. Wei, Simultaneously Decreasing the Bandgap and V_{oc} Loss in Efficient Ternary Organic Solar Cells, *Adv. Energy Mater.*, 2022, **12**, 2200129.

28 M. Li, S. Feng, S. Shen, H. Huang, W. Xue, N. Yu, Y. Zhou, W. Ma, J. Song, Z. Tang and Z. Bo, High efficiency ternary organic solar cells via morphology regulation with asymmetric nonfused ring electron acceptor, *Chem. Eng. J.*, 2022, **438**, 135384.

29 Z. Ling, M. I. Nugraha, W. T. Hadmojo, Y. Lin, S. Y. Jeong, E. Yengel, H. Faber, H. Tang, F. Laquai, A.-H. Emwas, X. Chang, T. Maksudov, M. Gedda, H. Y. Woo, I. McCulloch, M. Heeney, L. Tsetseris and T. D. Anthopoulos, Over 19% Efficiency in Ternary Organic Solar Cells Enabled by n-Type Dopants, *ACS Energy Lett.*, 2023, **8**, 4104–4112.

30 X. Li, A. Tang, H. Wang, Z. Wang, M. Du, Q. Guo, Q. Guo and E. Zhou, Benzotriazole-Based 3D Four-Arm Small Molecules Enable 19.1% Efficiency for PM6:Y6-Based Ternary Organic Solar Cells, *Angew. Chem., Int. Ed.*, 2023, **62**, e202306847.

31 K. Zhou, K. Xian, R. Ma, J. Liu, M. Gao, S. Li, T. Liu, Y. Chen, Y. Geng and L. Ye, Correlating miscibility, mechanical parameters, and stability of ternary polymer blends for high-performance solar cells, *Energy Environ. Sci.*, 2023, **16**, 5052–5064.

32 S. H. K. Paleti, S. Hultmark, J. Han, Y. Wen, H. Xu, S. Chen, E. Järsvall, I. Jalan, D. R. Villalva, A. Sharma, J. I. Khan, E. Moons, R. Li, L. Yu, J. Gorenflot, F. Laquai, C. Müller and D. Baran, Hexanary blends: a strategy towards thermally stable organic photovoltaics, *Nat. Commun.*, 2023, **14**, 4608.

33 J. Fu, Q. Yang, P. Huang, S. Chung, K. Cho, Z. Kan, H. Liu, X. Lu, Y. Lang, H. Lai, F. He, P. W. K. Fong, S. Lu, Y. Yang, Z. Xiao and G. Li, Rational molecular and device design enables organic solar cells approaching 20% efficiency, *Nat. Commun.*, 2024, **15**, 1830.

34 T. A. Dela Peña, R. Ma, Z. Xing, Q. Wei, J. I. Khan, R. M. Young, Y. Hai, S. A. Garcia, X. Zou, Z. Jin, F. L. Ng, K. L. Yeung, D. F. Swearer, M. R. Wasielewski, J. Wang, H. Cha, H. Yan, K. S. Wong, G. Li, M. Li and J. Wu, Interface property–functionality interplay suppresses bimolecular recombination facilitating above 18% efficiency organic solar cells embracing simplistic fabrication, *Energy Environ. Sci.*, 2023, **16**, 3416–3429.

35 H. Bai, R. Ma, W. Su, T. A. D. Peña, T. Li, L. Tang, J. Yang, B. Hu, Y. Wang, Z. Bi, Y. Su, Q. Wei, Q. Wu, Y. Duan, Y. Li, J. Wu, Z. Ding, X. Liao, Y. Huang, C. Gao, G. Lu, M. Li, W. Zhu, G. Li, Q. Fan and W. Ma, Green-Solvent Processed Blade-Coating Organic Solar Cells with an Efficiency Approaching 19% Enabled by Alkyl-Tailored Acceptors, *Nano-Micro Lett.*, 2023, **15**, 241.

36 Z. Xu, K. S. Park and Y. Diao, What Is the Assembly Pathway of a Conjugated Polymer From Solution to Thin Films?, *Front. Chem.*, 2020, **8**, 583521.

37 G. Odian, *Principles of Polymerization*, John Wiley & Sons, Inc., New York, 3rd edn, 1991.

38 I. M. Kalogeras, Glass-Transition Phenomena in Polymer Blends, *Encyclopedia of Polymer Blends*, 2016, pp. 1–134.

39 S. R. Forrest, *Organic electronics: foundations to applications*, Oxford University Press, USA, 2020.

40 T. Holstein, Studies of polaron motion: Part I. The molecular-crystal model, *Ann. Phys.*, 1959, **8**, 325–342.

41 Z. Tu, G. Han and Y. Yi, Barrier-Free Charge Separation Enabled by Electronic Polarization in High-Efficiency Non-fullerene Organic Solar Cells, *J. Phys. Chem. Lett.*, 2020, **11**, 2585–2591.

42 F.-Z. Cui, Z. Chen, J.-W. Qiao, P. Lu, X. Du, W. Qin, H. Yin and X.-T. Hao, Vertical-Phase-Locking Effect in Efficient and

This journal is © The Royal Society of Chemistry 2025

Energy Environ. Sci., 2025, **18**, 10164–10179 | 10177

Stable All-Polymer-Hosted Solar Cells, *ACS Energy Lett.*, 2022, **7**, 3709–3717.

43 J. Chen, Z. Pei, B. Chai, P. Jiang, L. Ma, L. Zhu and X. Huang, Engineering the Dielectric Constants of Polymers: From Molecular to Mesoscopic Scales, *Adv. Mater.*, 2024, **36**, 2308670.

44 J. Wu, C.-Y. Liao, Y. Chen, R. M. Jacobberger, W. Huang, D. Zheng, K.-W. Tsai, W.-L. Li, Z. Lu, Y. Huang, M. R. Wasielewski, Y.-M. Chang, T. J. Marks and A. Facchetti, To Fluorinate or Not to Fluorinate in Organic Solar Cells: Achieving a Higher PCE of 15.2% when the Donor Polymer is Halogen-Free, *Adv. Energy Mater.*, 2021, **11**, 2102648.

45 S. Karuthedath, S. H. K. Paleti, A. Sharma, H. Yin, C. S. P. De Castro, S. Chen, H. Xu, N. Alshehri, N. Ramos, J. I. Khan, J. Martin, G. Li, F. Laquai, D. Baran and J. Gorenflot, Rationalizing the Influence of Tunable Energy Levels on Quantum Efficiency to Design Optimal Non-Fullerene Acceptor-Based Ternary Organic Solar Cells, *Adv. Energy Mater.*, 2023, **13**, 2203464.

46 Y. Zhang and G. Li, Functional Third Components in Nonfullerene Acceptor-Based Ternary Organic Solar Cells, *Acc. Mater. Res.*, 2020, **1**, 158–171.

47 K. Vandewal, K. Tvingstedt, A. Gadisa, O. Inganäs and J. V. Manca, Relating the open-circuit voltage to interface molecular properties of donor: acceptor bulk heterojunction solar cells, *Phys. Rev. B:Condens. Matter Mater. Phys.*, 2010, **81**, 125204.

48 T. A. Dela Peña, J. I. Khan, N. Chaturvedi, R. Ma, Z. Xing, J. Gorenflot, A. Sharma, F. L. Ng, D. Baran, H. Yan, F. Laquai and K. S. Wong, Understanding the Charge Transfer State and Energy Loss Trade-offs in Non-fullerene-Based Organic Solar Cells, *ACS Energy Lett.*, 2021, **6**, 3408–3416.

49 U. W. Pohl and U. W. Pohl, Electronic Properties of Organic Semiconductors, *Epitaxy of Semiconductors: Physics and Fabrication of Heterostructures*, 2020, pp. 177–205.

50 A. Köhler and H. Bässler, *Electronic processes in organic semiconductors: An introduction*, John Wiley & Sons, 2015.

51 S. Karuthedath, J. Gorenflot, Y. Firdaus, N. Chaturvedi, C. S. De Castro, G. T. Harrison, J. I. Khan, A. Markina, A. H. Balawi, T. A. Dela Peña, W. Liu, R.-Z. Liang, A. Sharma, S. H. K. Paleti, W. Zhang, Y. Lin, E. Alarousu, S. Lopatin, D. H. Anjum, P. M. Beaujuge, S. De Wolf, I. McCulloch, T. D. Anthopoulos, D. Baran, D. Andrienko and F. Laquai, Intrinsic efficiency limits in low-bandgap non-fullerene acceptor organic solar cells, *Nat. Mater.*, 2021, **20**, 378–384.

52 F. Eisner, G. Foot, J. Yan, M. Azzouzi, D. G. Georgiadou, W. Y. Sit, Y. Firdaus, G. Zhang, Y.-H. Lin, H.-L. Yip, T. D. Anthopoulos and J. Nelson, Emissive Charge-Transfer States at Hybrid Inorganic/Organic Heterojunctions Enable Low Non-Radiative Recombination and High-Performance Photodetectors, *Adv. Mater.*, 2022, **34**, 2104654.

53 U. Hörmann, S. Zeiske, F. Piersimoni, L. Hoffmann, R. Schlesinger, N. Koch, T. Riedl, D. Andrienko and D. Neher, Stark effect of hybrid charge transfer states at planar ZnO/organic interfaces, *Phys. Rev. B*, 2018, **98**, 155312.

54 X. Liu, K. Ding, A. Panda and S. R. Forrest, Charge Transfer States in Dilute Donor–Acceptor Blend Organic Heterojunctions, *ACS Nano*, 2016, **10**, 7619–7626.

55 P. W. Atkins, J. De Paula and J. Keeler, *Atkins' physical chemistry*, Oxford University Press, 2023.

56 F. D. Eisner, M. Azzouzi, Z. Fei, X. Hou, T. D. Anthopoulos, T. J. S. Dennis, M. Heeney and J. Nelson, Hybridization of local exciton and charge-transfer states reduces nonradiative voltage losses in organic solar cells, *J. Am. Chem. Soc.*, 2019, **141**, 6362–6374.

57 D. Qian, S. M. Pratik, Q. Liu, Y. Dong, R. Zhang, J. Yu, N. Gasparini, J. Wu, T. Zhang, V. Coropceanu, X. Guo, M. Zhang, J.-L. Bredas, F. Gao and J. R. Durrant, Correlating the Hybridization of Local-Exciton and Charge-Transfer States with Charge Generation in Organic Solar Cells, *Adv. Energy Mater.*, 2023, **13**, 2301026.

58 T. A. Dela Peña, J. I. Khan, N. Chaturvedi, R. Ma, Z. Xing, J. Gorenflot, A. Sharma, F. L. Ng, D. Baran, H. Yan, F. Laquai and K. S. Wong, Understanding the Charge Transfer State and Energy Loss Trade-offs in Non-fullerene-Based Organic Solar Cells, *ACS Energy Lett.*, 2021, **6**, 3408–3416.

59 Z. Chen, X. Chen, Z. Jia, G. Zhou, J. Xu, Y. Wu, X. Xia, X. Li, X. Zhang, C. Deng, Y. Zhang, X. Lu, W. Liu, C. Zhang, Y. Yang and H. Zhu, Triplet exciton formation for non-radiative voltage loss in high-efficiency nonfullerene organic solar cells, *Joule*, 2021, **5**, 1832–1844.

60 A. Rao, P. C. Y. Chow, S. Gélinas, C. W. Schlenker, C.-Z. Li, H.-L. Yip, A. K. Y. Jen, D. S. Ginger and R. H. Friend, The role of spin in the kinetic control of recombination in organic photovoltaics, *Nature*, 2013, **500**, 435–439.

61 J. Wong, S. T. Omelchenko and H. A. Atwater, Impact of Semiconductor Band Tails and Band Filling on Photovoltaic Efficiency Limits, *ACS Energy Lett.*, 2021, **6**, 52–57.

62 H. Bin, Y. Yang, Z.-G. Zhang, L. Ye, M. Ghasemi, S. Chen, Y. Zhang, C. Zhang, C. Sun, L. Xue, C. Yang, H. Ade and Y. Li, 9.73% Efficiency Nonfullerene All Organic Small Molecule Solar Cells with Absorption-Complementary Donor and Acceptor, *J. Am. Chem. Soc.*, 2017, **139**, 5085–5094.

63 X. Yuan, Y. Zhao, Y. Zhang, D. Xie, W. Deng, J. Li, H. Wu, C. Duan, F. Huang and Y. Cao, Achieving 16% Efficiency for Polythiophene Organic Solar Cells with a Cyano-Substituted Polythiophene, *Adv. Funct. Mater.*, 2022, **32**, 2201142.

64 G. Cai, Y. Li, Y. Fu, H. Yang, L. Mei, Z. Nie, T. Li, H. Liu, Y. Ke, X.-L. Wang, J.-L. Brédas, M.-C. Tang, X. Chen, X. Zhan and X. Lu, Deuteration-enhanced neutron contrasts to probe amorphous domain sizes in organic photovoltaic bulk heterojunction films, *Nat. Commun.*, 2024, **15**, 2784.

65 G. Dunér, E. Thormann and A. Dėdinaitė, Quartz Crystal Microbalance with Dissipation (QCM-D) studies of the viscoelastic response from a continuously growing grafted polyelectrolyte layer, *J. Colloid Interface Sci.*, 2013, **408**, 229–234.

66 A. D. Easley, T. Ma, C. I. Eneh, J. Yun, R. M. Thakur and J. L. Lutkenhaus, A practical guide to quartz crystal microbalance with dissipation monitoring of thin polymer films, *J. Polym. Sci.*, 2022, **60**, 1090–1107.

10178 | *Energy Environ. Sci.*, 2025, **18**, 10164–10179

This journal is © The Royal Society of Chemistry 2025

67 A. Devižis, A. Gelzinis, J. Chmeliov, M. Diethelm, L. Endriukaitis, D. Padula and R. Hany, Carrier Tunneling from Charge Transfer States in Organic Photovoltaic Cells, *Adv. Funct. Mater.*, 2021, **31**, 2102000.

68 C. Deibel, T. Strobel and V. Dyakonov, Role of the charge transfer state in organic donor–acceptor solar cells, *Adv. Mater.*, 2010, **22**, 4097–4111.

69 P. Krauspe, D. Tsokkou, M. Causa, E. Buchaca-Domingo, Z. Fei, M. Heeney, N. Stingelin and N. Banerji, Terahertz short-range mobilities in neat and intermixed regions of polymer:fullerene blends with controlled phase morphology, *J. Mater. Chem. A*, 2018, **6**, 22301–22309.

70 J. M. de la Perrelle, R. J. Hudson, A. Dolan, S. Jana, X. Pan, M. R. Andersson, H.-S. Tan, Z. H. Alotaibi, G. G. Andersson, T. A. Smith, D. M. Huang and T. W. Kee, From light to hydrogen: the complete life cycle of free charges in photo-catalytic nanoparticles, *Sustainable Energy Fuels*, 2024, **8**, 3145–3163.

71 M. B. Price, P. A. Hume, A. Ilina, I. Wagner, R. R. Tamming, K. E. Thorn, W. Jiao, A. Goldingay, P. J. Conaghan, G. Lakhwani, N. J. L. K. Davis, Y. Wang, P. Xue, H. Lu, K. Chen, X. Zhan and J. M. Hodgkiss, Free charge photo-generation in a single component high photovoltaic efficiency organic semiconductor, *Nat. Commun.*, 2022, **13**, 2827.

72 X. Ai, M. C. Beard, K. P. Knutsen, S. E. Shaheen, G. Rumbles and R. J. Ellingson, Photoinduced charge carrier generation in a poly (3-hexylthiophene) and methanofullerene bulk heterojunction investigated by time-resolved terahertz spectroscopy, *J. Phys. Chem. B*, 2006, **110**, 25462–25471.

73 K. Ohta, K. Tominaga, T. Ikoma, Y. Kobori and H. Yamada, Microscopic Structures, Dynamics, and Spin Configuration of the Charge Carriers in Organic Photovoltaic Solar Cells Studied by Advanced Time-Resolved Spectroscopic Methods, *Langmuir*, 2022, **38**, 7365–7382.

74 A. J. Gillett, A. Privitera, R. Dilmurat, A. Karki, D. Qian, A. Pershin, G. Londi, W. K. Myers, J. Lee, J. Yuan, S.-J. Ko, M. K. Riede, F. Gao, G. C. Bazan, A. Rao, T.-Q. Nguyen, D. Beljonne and R. H. Friend, The role of charge recombination to triplet excitons in organic solar cells, *Nature*, 2021, **597**, 666–671.

75 S.-i Natsuda, T. Saito, R. Shirouchi, Y. Sakamoto, T. Takeyama, Y. Tamai and H. Ohkita, Cascaded energy landscape as a key driver for slow yet efficient charge separation with small energy offset in organic solar cells, *Energy Environ. Sci.*, 2022, **15**, 1545–1555.

This journal is © The Royal Society of Chemistry 2025

Energy Environ. Sci., 2025, **18**, 10164–10179 | 10179